CORROSION SCIENCE AND TECHNOLOGY, Vol.7, No.2(2008), pp.69~76

High Temperature Corrosion in Carbon-Rich Gases

D.J. Young

School of Materials Science and Engineering, University of New South Wales
UNSW, Sydney, NSW 2033, Australia

Common methods for large scale hydrogen production, such as steam reforming and coal gasification, also involve production of carbonaceous gases. It is therefore necessary to handle process gas streams involving various mixtures of hydrocarbons, H_2, H_2O, CO and CO_2 at moderate to high temperatures. These gases pose a variety of corrosion threats to the alloys used in plant construction. Carbon is a particularly aggressive corrodent, leading to carburisation and, at high carbon activities, to metal dusting. The behaviour of commercial heat resisting alloys 602CA and 800, together with that of 304 stainless steel, was studied during thermal cycling in CO/CO_2 at 650-750℃, and also in $CO/H_2/H_2O$ at 680℃. Thermal cycling caused repeated scale separation, which accelerated chromium depletion from the alloy subsurface regions. The $CO/H_2/H_2O$ gas, with a_C=2.9 and $p(O_2)=5x10^{-23}$ atm, caused relatively rapid metal dusting, accompanied by some internal carburisation. In contrast, the CO/CO_2 gas, with a_C=7 and $p(O_2)=10^{-23}$-10^{-24} atm caused internal precipitation in all three alloys, but no dusting. Inward diffusion of oxygen led to *in situ* oxidation of internal carbides. The very different reaction morphologies produced by the two gas mixtures are discussed in terms of competing gas-alloy reaction steps.

Keywords *: internal oxidation, carburisation, coking, catalysis, dusting*

1. Introduction

Common methods for the large scale production of hydrogen, such as steam reforming and coal gasification, also involve production of carbonaceous gases. The key reactions can be summarised as

$$CH_4 + H_2O = CO + 3H_2 \quad (1)$$

$$C(s) + H_2O = CO + H_2 \quad (2)$$

$$CO + H_2O = CO_2 + H_2 \quad (3)$$

The off gases are processed further (for cleaning and temperature adjustment) and the further reactions

$$2CO = CO_2 + C \quad (4)$$

$$CO_2 = CO + \tfrac{1}{2}O_2 \quad (5)$$

must be considered.

At the moderate temperature involved, these gases can be both oxidising and carburising to chromia-forming alloys. Even under conditions where Cr_2O_3 is stable, the carbon can nonetheless cause damage in a number of ways. Carbon can penetrate chromia scales, causing internal carburisation of the underlying alloy.[1)-5)] The development of an internal oxidation zone together with a deeper carburisation zone has also been observed.[4),6)-8)] Gases with unit carbon activity can deposit coke if they contact chromium depleted metal revealed by scale spallation.[8)] In addition, breakaway oxidation of 9% chromium steels has been shown[9)] to result from carbon deposition via the Boudouard reaction, Eqn (4), at the scale-metal interface. Finally, the possibility of metal dusting exists if $a_C>1$,[10),11)] a situation which can arise at moderate temperatures because reaction (4) and the reverse of reaction (2) are slow.

The ability of an alloy to form a chromia scale depends on the chromium concentration available at the alloy surface. This concentration will be lower than that of the bulk alloy if internal precipitation of chromium-rich compounds occurs. It is also reduced by repeated cycles of selective Cr_2O_3 scale formation and spallation.

The present work was intended to provide information on corrosion of chromia-forming alloys under conditions where Cr_2O_3 is stable, but the gas is supersaturated with respect to carbon. Temperature cycling was used to accelerate alloy chromium depletion, a procedure which has

† Corresponding author: d.young@unsw.edu.au

been shown[14] to accelerate metal dusting.

2. Experimental

The three commercial alloys shown in Table 1 were investigated. Compositions are stated in w/o, weight percent. Sample coupons of dimension 10 x 10 x 2 mm were cut from as-received stock and then prepared with two surface finishes. Surfaces were either mechanically ground to an 800 grit finish or subsequently chemically etched in 75% concentrated hydrochloric acid, 25% concentrated nitric acid. The latter treatment removed the work hardened surface region of the alloys and produced a pitted surface. The alloys were exposed at temperatures of 650, 700 and 750℃ to flowing CO-CO_2 gas mixtures of the compositions listed in Table 2. All gases were supersaturated with respect to carbon, as calculated from the equilibrium of reaction (4).

As carbon was not deposited on inert surfaces within the reaction apparatus, it is concluded that equilibrium was not achieved, and the gases remained supersaturated. Oxygen potentials were calculated from the equilibrium of reaction (5) and the results are listed in Table 2. Comparison of these values with those calculated for oxidation equilibria showed that both gases were oxidising to Al, Cr, Mn and Si, but not Fe or Ni. Temperature cycling was achieved by driving an electrically heated furnace at periodic intervals between two positions: one corresponding to the samples being located in the furnace hot zone and the other to the samples being outside the furnace. The cyclic operation was automatically controlled, consisted of 45 min at reaction temperature and 15 min at ambient, and was repeated up to 528 times. Alloy samples were weighed initially and from time to time during the course of each experiment.

Table 1. Alloy compositions (w/o)

Alloy	Fe	Ni	Cr	Mn	Si	Other
800H	Bal	32.7	20.4	0.69	0.43	0.48Ti, 0.31Al
SS304	Val	8.7	17.6	0.83	0.55	
602CA	9.2	Bal	25.1	0.08	0.05	0.13Ti, 2.28Al;0.09Y

The effects of hydrogen were investigated by using a gas mixture of CO-26H_2-6H_2O (vol. pct.), corresponding to a_C=2.9and $p(O_2)=10^{-23}$ atm at T=680℃. In these experiments, coke was deposited on the sample surfaces, but not on the reactor walls. Surface deposits were collected and weighed, and the decreased weight of alloy remaining after reaction was also determined. Reaction products were examined using conventional analytical techniques.

3. Results

3.1 Reaction with CO/CO_2

Weight change kinetics at 700℃ are shown in Fig. 1. The results are net values representing both weight gained (due to carbon and oxygen uptake) and weight losses due to scale spallation or alloy surface disintegration. Similar results were obtained at 650 and 750℃.[12] Chemically etched materials always gained more weight than the corresponding ground samples. Type 304 stainless steel always gained more weight than the nickel alloys, and 602CA was generally the least reactive.

Analysis by X-ray diffraction (XRD) of reacted alloy surfaces showed that chromia was formed in all cases except ground 602CA, on which no product of any sort was detected. Spinel was formed on SS304 and alloy 800. Iron and chromium carbides were detected on SS304 only. No graphite was detected by XRD on any reacted surface.

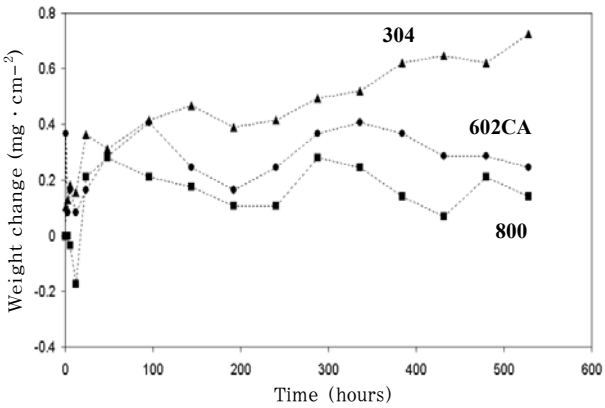

Fig. 1. Cyclic reaction in CO/CO_2 at 700℃

Table 2. Reaction gas mixtures

	Input gas (vol%)					Equilibrium activities	
	CO	CO_2	H_2	H_2O	Ar	a_c	$P(O_2)$/atm
CO/CO_2 (700℃)	7.0	1.0			92.0	7.0	$1x10^{-23}$
$CO/H_2/H_2O$(680℃)	58.0		26.0	6.0		2.9	$5x10^{-23}$

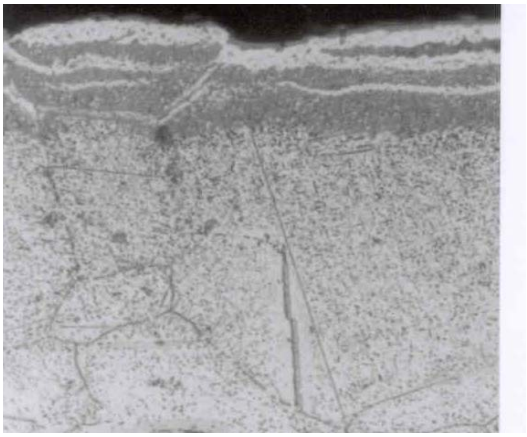

Fig. 2. Type 304 stainless after cycling in CO/CO_2

A cross-section of reacted 304 stainless is shown in Fig. 2, where scale damage and spallation is evident. The roughened etched surfaces retained more scale than the ground ones, and had started to disintegrate. All alloys had sustained internal attack, the severity of the damage being generally greater for the etched surfaces.

Internal attack was most severe in SS304. Two zones of precipitates were identified: oxide in the subsurface zone and carbides at greater depths. The oxides were identified[12] as spinel near the surface with Cr_2O_3 beneath. Alloy 800 developed intergranular oxides and fine intragranular carbides. Alloy 602CA formed intergranular carbides, but very little intragranular carburisation occurred. Instead, a shallow zone of internal intragranular oxidation developed.

3.2 Reaction in $CO/H_2/H_2O$

Carbon was found to have deposited on electropolished alloys and the kinetics of deposit accumulation are shown in Fig. 3. Mass changes in the substrate alloys after deposit removal are shown in Fig. 4. These reflect the net result of mass increases due to oxidation and carburisation, and mass loss due to scale spallation and/or metal dusting.

The carbon deposits were found to be filamentary, containing austenite particles at their tips (Fig. 5). Examination by transmission electron microscopy[15] has confirmed that the filaments were multi-wall carbon nanotubes. Phases found in the deposits using XRD were graphite, austenite, spinel and M_7C_3.

Metallographic cross-sections (Fig. 6) showed that the alloy surfaces had been pitted. External carbon deposition and dusting along with internal precipitation of chromium-rich carbides were associated with the pitting. Unattacked regions of the alloy surface were covered by oxide scale. Carburisation and surface recession quickly became general on Alloy 800.

Ground alloy surfaces were much more resistant to attack. No coking or mass loss was observed for 602CA up to 1200 cycles, and the only reaction product was Cr_2O_3

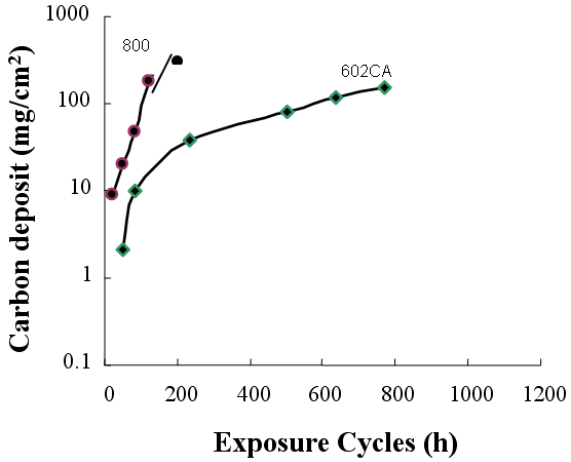

Fig. 3. Mass uptake in $CO/H_2/H_2O$ at 680℃

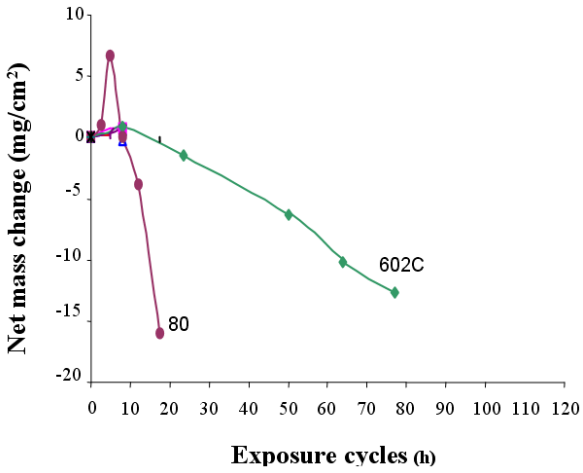

Fig. 4. Alloy mass loss in $CO/H_2/H_2O$ at 680℃

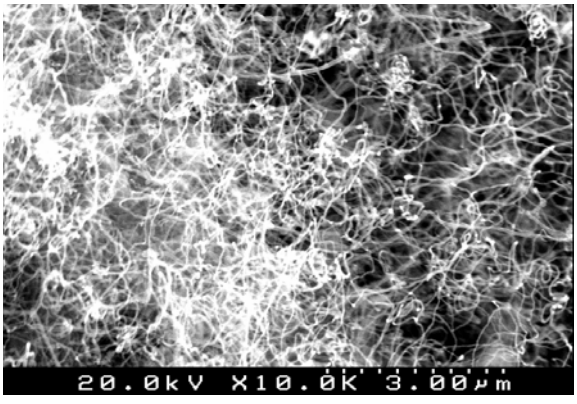

Fig. 5. SEM image of filamentary coke deposited from $H_2/CO/H_2O$

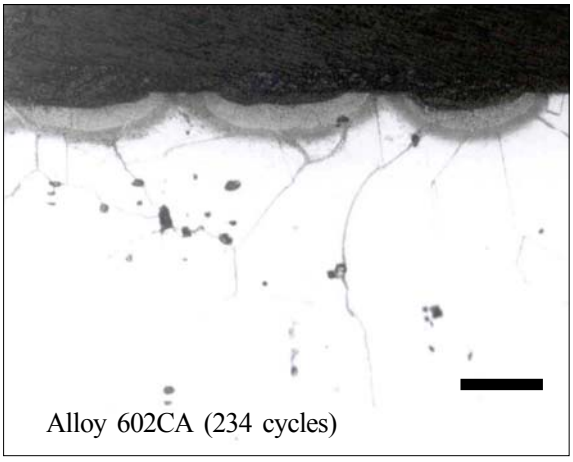

Fig. 6. Dusting attack in $H_2/CO/H_2O$

scale. Alloy 800 was attacked, but the onset of dusting was delayed until 370 cycles. The coke deposit formed on the ground surface was similar to that on electropolished 800.

4. Discussion

The two sets of reaction conditions used corresponded to almost identical carbon activities (7 and 3) and rather similar oxygen potentials (1 and $5x10^{-23}$ atm) if gas phase equilibrium of reactions (3) and (4) is assumed. Both gases were therefore oxidising to Cr, Al and Si, but not to iron or nickel; both were carbon supersaturated with respect to graphite, and capable of forming chromium and iron carbides.

Reacted alloys showed qualitatively similar patterns of internal precipitation and oxide scaling after exposure to both gases, but dramatically different extents of carbon deposition and metal disintegration. The two forms of corrosion are considered separately.

4.1 Internal precipitation and oxide scaling

Selective oxidation of chromium led in all cases (except perhaps ground 602CA in CO/CO_2) to the growth of external scales consisting mainly of Cr_2O_3. In addition, some spinel, MCr_2O_4, was formed on the lower chromium content alloys, SS304 and Alloy 800H, via the reaction

$$M + Cr_2O_3 + \tfrac{1}{2}O_2 = MCr_2O_4 \quad (7)$$

The selective removal of chromium from the alloys led to a lowering of chromium concentration in the alloy. Repeated thermal cycles subjected the alloy-scale composite structures to mechanical stress, leading to scale damage. The resulting scale breakage and spallation were evident in the periodic weight losses (Fig. 1), and the appearance of the remnant surface reaction products. The weight losses were obscured in the H_2/CO reaction cases by the much larger weight uptake due to carbon deposition (Fig. 3). This repeated mechanical damage to the scales destroyed their protective capability and exposed the underlying alloys to the gas and renewed oxidation. Each cycle of damage therefore led to further selective removal of chromium from the alloy.

At the reaction temperatures studied, metal diffusion within the alloys was slow. Removal of chromium from the alloy subsurface regions therefore could not be compensated by a diffusive flow from the alloy interior. Under these circumstances, repeated scale damage events led to further lowering of the chromium concentration at the alloy surface until not enough remained to reform an external Cr_2O_3 scale, and the alloys became vulnerable to internal attack.

Much smaller amounts of scale were found on 602CA than the other alloys. None was visible by optical metallography on ground surfaces, but thin layers were seen on etched surfaces reacted in both cases. The better retention of these scales may have been related to the simultaneous occurrence of internal oxidation.

Once the ability of an alloy to reform protective chromia was lost, gas access to the metal surface led to dissolution and inward diffusion of carbon and oxygen. Both could react with alloy solute chromium to form internal precipitates

$$2Cr + 3O = Cr_2O_3 \quad (8)$$

$$23Cr + 6C = Cr_{23}C_6 \quad (9)$$

$$7Cr_{23}C_6 + 27C = 23Cr_7C_3 \quad (10)$$

The development of oxide precipitate was studied only in the case of SS304 reacted with CO/CO2 gas, where massive intragranular oxidation occurred. The location of the oxides immediately beneath the surface, with the carbides at greater depth, is as expected.[8),16)] It reflects the fact that the reaction

$$2Cr_7C_3 + 21O = 7Cr_2O_3 + 6C \quad (11)$$

is thermodynamically favoured at high dissolved oxygen concentrations which existed near the surface, but not at greater depths. The further formation of spinel just beneath the alloy surface resulted from reaction (7) occurring within the alloy as a result of even higher dissolved oxygen concentrations so near the surface.

Table 3. Measured internal carburisation depths/μm

Alloy	CO/CO_2	$CO/H_2/H_2O$
304	520	n/d
800	440	96
602CA	0	49

The kinetics of internal precipitation were not studied, but qualitative information is available from the metallography. Carburisation depths measured from cross-sections of reacted alloys are summarised in Table 3. The relative rates of internal carburisation are expected to reflect the rate of inward carbon diffusion. Precipitation depths X are on this basis predicted[13] to increase parabolically with time:

$$X^2 = 2k_p t \tag{12}$$

$$k_p = \frac{\varepsilon D_C N_C}{\nu N_{cr}} \tag{13}$$

where k_p is the rate constant, t time, D_C the diffusion coefficient of carbon and N_C its surface concentration, N_{Cr} the original alloy chromium content, ε a diffusional blocking factor and ν the stoichiometry of CrC_ν. Intragranular carbide precipitation occurs by volume diffusion of dissolved carbon, and rates should be predictable using Eq. (13).

Extrapolation of high temperature date for N_C, D_C leads to the prediction[14] that Alloy 800 and SS304 will carburise at about the same rates at 700℃, and 602CA at a rate 3 to 4 times slower. The scant data in Table 3 is only very approximately in accord with these predictions. Since the carbon permeability of 602CA is relatively high, it is concluded from the lack of internal carburisation of this alloy in CO/CO_2 that carbon dissolution was blocked by the external scale. It is likely that some alumina formation on this alloy contributed to this success.

Comparative data (Table 3) for carburisation rates of the alloys 800 and 602CA in the two gases is difficult to understand on the basis of Eqn (13). The value of k_p for Alloy 800 reacted with CO/CO_2 is about 10 times the corresponding value for the H_2/CO reaction. Given that the value of a_C for the former gas is calculated to be only about twice that in the latter, this result is surprising. Furthermore, 602CA carburises in the low carbon activity gas, but not at high carbon activity. The oxygen potential of the low a_C gas is somewhat higher than in the high a_C gas, perhaps favouring internal Al_2O_3 precipitation over scaling. However, internal oxidation was observed after reaction with CO/CO_2. It is concluded on this basis that the equilibrium a_C and $p(O_2)$ values calculated for the two gases do not provide a satisfactory explanation of the observed differences in alloy corrosion.

4.2 Carbon deposition and metal disintegration

Reactions with the two gases produced dramatically different results. Whereas the H_2/CO gas deposited large amounts of carbon on the surface and caused metal dusting, the CO/CO_2 gas produced no carbon deposit, and led to a different form of metal disintegration.

The general mechanism of the dusting reaction apparent in the present results is largely consistent with that of earlier work. Thus, the alloys resisted carbon attack for so long as an oxide scale was retained. Chromia and alumina are impermeable to carbon[17] and an adherent layer of either Cr_2O_3 or Al_2O_3 will protect an alloy from carbon attack.[19] Neither oxide is catalytic to coking, and no carbon deposition from the supersaturated gas occurs whilst the alloy scales are intact.

As noted earlier, thermal cycling led to chromium depletion and the onset of internal precipitation. This caused further lowering of the metal matrix chromium, and the reformation of a protective scale became impossible. In the H_2/CO atmosphere, reaction between the gas and the remnant iron and nickel enriched metal then led to carbon deposition and metal dusting. Carbon always deposited as filaments which were actually multi-wall graphite nanotubes. The growth of these tubes at such low temperatures is attributed to catalysis by the particles present at the filament tips.[15),18),22] In the case of these austenitic materials, the catalytically active particles were nickel-rich austenite, in agreement with earlier models.

The mechanism whereby carbon causes dusting of austenitic alloys is not yet completely clear. However, it certainly involves nucleation and growth of graphite at or beneath the metal surface.[22)-24] For graphite to grow into the metal requires that carbon dissolve in the austenite and diffuse to the advancing graphite front. The flux of dissolved carbon is expected to be related to the permeability, which depends on the Fe/Ni ratio[20),21] in the chromium-depleted alloy. Carbon permeability in the relatively high iron content Alloy 800 will be grater than in 602CA, thereby explaining the relative dusting rates for these two alloys shown in Fig. 5.

When the same alloys were exposed to the CO/CO_2 gas however, no graphite deposition occurred and no finely divided metal particles (dust) were formed. The calculated equilibrium carbon activities and oxygen potentials of the gases (Table 2) do not explain this result, just as they fail to rationalise the differing patterns of internal preci-

pitation.

Since the gas mixtures are not at equilibrium, it is perhaps not surprising that carbon and oxygen potentials calculated on the supposition of equilibrium are not consistent with experimental observation. It has recently been demonstrated[24] that variation with changing gas composition in the rate of coke accumulation on pure nickel is similarly at variance with prediction based on equilibrium. Instead, a kinetic description based on independent reactions

$$CO + H_2 \rightarrow H_2O + C \quad (a)$$

$$2CO \rightarrow CO_2 + C \quad (b)$$

$$CH_4 \rightarrow 2H_2 + C \quad (c)$$

leading to the rate equation

$$Rate = k_a p_{CO} p_{H2} + k_v p_{CO_2}^2 - k_c p_{H_2}^2 \quad (14)$$

was shown to succeed. Neglecting carbon gasification by H_2O and CO_2, but including methane formation led to estimates at 680℃ of k_a=0.72, k_b=0.061 and k_c=0.274 mg cm^{-2} atm^{-2} h^{-1}. The finding that reaction (a) was faster than reaction (b) is in agreement with earlier work.[25] Assuming that similar values apply to the nickel-rich matrices of chromium-depleted alloys 800 and 602CA, and ignoring any changes arising from the small temperature difference, the rates shown in Table 4 are calculated for the two gas mixtures.

Comparison of the ratio predicted for the H_2/CO gas mixture with the measured kinetics shown in Fig. 4 shows that order of magnitude agreement is achieved for the nickel-base 602CA. Clearly the model does not apply to Alloy 800, a failure which can be attributed to the high iron content of this alloy, and the consequently different catalytic activity to reactions (a) and (b).

The difference in carbon deposition rates in the two gas atmospheres is now seen to be due to the much faster rate of the hydrogen-carbon monoxide reaction. The rate of carbon production in the CO/CO_2 gas was presumably slow enough for all the carbon to dissolve into the alloy, and no measurable graphite deposit resulted.

Table 4. Predicted coking rates/ mg cm^{-2} h^{-1}

	$k_a p_{CO} p_{H2} + k_b p_{CO_2}^2 - k_c p_{H_2}^2$		
H_2/CO	0.13	0.03	0.001
CO/CO_2	0	$3x10^{-4}$	0

Table 5. Calculated effects of complete chromium precipitation

Precipitate	f_V	ΔV/%
$FeCr_2O_4$	0.45	40
Cr_2O_3	0.32	21
Cr_7C_3	0.21	3
$Cr_{23}C_7$	0.20	3

The differences in Alloy 800 internal carburization rates in the two gases (Table 4) can be explained in similar terms. The H_2/CO reaction kinetics were such as to produce large quantities of surface graphite, which is unable to dissolve in the alloy. The quantity of dissolved carbon was consequently low. The CO/CO_2 reaction produced little or no surface graphite, and essentially all of the product carbon was dissolved in the alloy, carburizing it to a greater depth.

The association of graphite deposition with metal dusting of alloys 800 and 602CA is clear. Both processes took place in the H_2/CO gas, but neither occurred in CO/CO_2. In the latter case a different form of metal disintegration was seen to lead to the detachment of coarse metal particles from the alloy surface. An enlarged view of the surface is shown in Fig. 7.

As discussed above, reaction of the alloys with CO/CO_2 led to the injection of significant amounts of carbon and precipitation of internal chromium-rich carbides. Further subsequent oxidation of the remaining alloy chromium and *in situ* conversion of the carbide precipitates to oxides led to significant volume expansion. Considering the internal precipitates in SS304, adopting the approximation that all alloy chromium was precipitated and using molar volumes of 29.1, 45.0, 54.8 and 181.9 cm^3 $mole^{-1}$ for Cr_2O_3,

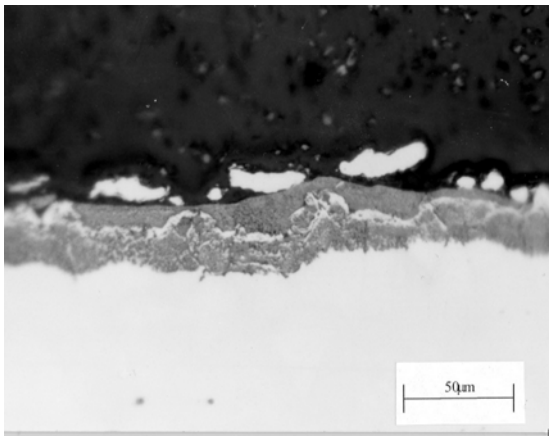

Fig. 7. Surface disintegration of 304 stainless after cyclic CO/CO_2 reaction

$FeCr_2O_4$, Cr_7C_3 and $Cr_{23}C_6$, respectively, the volume fraction within the steel (density 7.9 g cm^{-3}) can be calculated. Results are shown in Table 5, along with the expected volume expansions. These figures explain why large volume fractions of internal carbides can precipitate within austenite.

Similar quantities of internal oxide cannot normally form, an external scale developing instead. Because the presently studied reaction conditions led to prior internal precipitation of chromium as carbide, subsequent oxidation led to *in situ* conversion of the precipitates, and formation of a very large internal oxide volume fraction. The mechanical stress associated with this change would have been exacerbated by thermal cycling. It is therefore suggested that mechanical failure, rather than carbon deposition, led to the surface damage observed after reaction with CO/CO_2.

It is recognized from the foregoing discussion that the effective carbon activity at the alloy surface is unknown. Surface deposition of coke from the H_2/CO mixture removed substantial amounts of carbon from the gas phase into a form which played no part in attacking the underlying alloy, thereby reducing a_C. On the other hand, removal of oxygen to form Cr_2O_3 or spinel increases the local CO/CO_2 ratio, thereby increasing a_C. However, it seems from the success of the rate equation (14) that the concept of an equilibrium carbon activity lacks physical significance under the conditions used. Nonetheless, it can be concluded that reaction (a) injects carbon into the alloys at a rapid rate, leading to supersaturation with respect to graphite, precipitation of that phase, and consequent metal dusting. Similarly, it is concluded that reaction (b) dissolves carbon into the alloys at a rate which can be accommodated by inward alloy diffusion and consequent internal carburisation.

4.3 Effect of surface condition

High-temperature annealing followed by electropolishing produced alloy surface regions which were coarse grained and free of deformation. Subsurface mass transport was therefore controlled by lattice diffusion. Cold working the alloy surface increased dislocation densities and, after recrystallisation, led to a finer grain size, resulting in accelerated subsurface diffusion. Protective scale formation and rehealing capacity are then improved[28] and long-term resistance to dusting is known to be enhanced.[26-28] The same benefit would be expected during rapid thermal cycling, as was in fact observed.

Alloy reactions with CO/CO_2 were affected in the same way. Chemical etching removed the work hardened region present beneath ground surfaces. Damaged oxide scales were more slowly repaired on the etched surfaces than on ground ones, accounting for the greater extent of internal precipitation beneath the former.

5. Conclusions

Thermal cycling of three chromia-forming alloys in both CO/CO_2 and H_2/CO atmospheres caused scale spallation and gas access to the underlying metal. At the low oxygen pressures of these atmospheres, chromium was selectively oxidised and depleted from the alloy subsurface region. Inward diffusion of carbon and oxygen then led to internal precipitation of near surface oxides and deeper carbides. The fast reaction between CO and H_2 led to surface coking, graphitization and metal dusting, accompanied by relatively slow internal carburization. The slower Boudouard reaction produced no coking, graphitization or metal dusting, but more extensive internal carburization. This pattern of reaction products was inconsistent with gas phase carbon and oxygen potentials calculated on the assumption of equilibrium. It is concluded that the equilibrium assumption is misleading, and that a description based on parallel but independent gas-alloy reaction paths is more realistic.

Acknowledgement

Support for this work by the Australian Research Council is gratefully acknowledged.

References

1. H. E. McCoy, *Corrosion*, **21**, 84 (1965).
2. F. S. Pettit, J. A. Goebel, G. W. Goward, *Corros. Sci*., **9**, 903 (1969).
3. G. H. Meier, W. C. Coons, R. A. Perkins, *Oxid. Met*., **17**, 235 (1982).
4. J. A. Colwell and R. A. Rapp, *Met. Trans*. A **17A**, 1065 (1986).
5. X. G. Zheng, D. J. Young, Mater, Sci. Forum **251-4**, 567 (1997).
6. P. R. S. Jackson, D. J. Young, and D. L. Trimm, *J. Mater. Sci*., **21**, 4376 (1986).
7. J. Perkins and A. Goldberg, *Oxid. Met.*, **11**, 23 (1977).
8. D. J. Young and S. Watson, *Oxid. Met*., **44**, 239 (1955).
9. G. B. Gibbs, *Oxid. Met*., **7**, 173 (1973).
10. R. F. Hochman, Proc. 4th Int. Cong. Met. Corrosion, p. 258, NACE, Houston (1972).
11. J. C. Nava Paz and H. J. Grabke, *Oxid. Met.*, **39**, 437 (1993).
12. M. Hansel, C. Boddington, D.J. Young, *Corros. Sci*., **45**, 967 (2003).
13. C. Wagner, *Z. Electrochem*., **63**, 772 (1959).
14. C. H. Toh, P. R. Munroe, D. J. Young, K. Foger, *Mater.*

High Temp. **20**, 129 (2003).
15. C. H. Toh, P. R. Munroe, D. J. Young, *Oxid. Met*., **28** (2000)
16. C. S. Giggins and F. S. Pettit, *Oxid. Metals*, **14**, 363 (1980).
17. H. J. Grabke, K. Ohla, J. Peters, I. Wolf, Werkst. Korros., **34**, 495 (1983).
18. R. T. K. Baker, M. A. Barker, P. S. Harris, F. S. Yeates, R. J. Waite, J. Catal., **26**, 51 (1972).
19. R. Schneider, E. Pippel, J. Woltersadorf, S. Strauss, H. J. Grabke, *Mater. Technol*., **68**, 326 (1997).
20. T. Wada, H. Weda, I. F. Elliott, J. Chipman, *Met. Trans*., **2**, 2199 (1971).
21. S. K. Bose, H. J. Grabke, *Z. Metall*., **69**, 8 (1978).
22. J. C. Nava Paz and H. J. Grabke, *Oxid. Met*., **39**, 437 (1993).
23. C. M. Chun, J. D. Mumford and T. A. Ramanarayanan, *J. Electrochem. Soc.*, **147**, 3680 (2000).
24. J. Zhang and D. J. Young, *Corros. Sci*., **49**, 1496 (2007).
25. S. Leistikow, *Mater. Chem*., **1**, 189 (1976).
26. H. J. Grabke, R. Krajak, E. M. Müller-Lorenz, S. Strauss, *Mater Corros*., **47**, 495 (1996).
27. H. J. Grabke, R. Krajak, E. M. Müller-Lorenz, B. Ekter, M. Lucas, D. Monceau, *Steel Research*, **68**, 179 (1997).
28. H. J. Grabke, R. Krajak, E. M. Müller-Lorenz, J. Klöwer, D. C. Agarwal, *Mat. Performance*, **27**, 7 (1998).